Available online at www.sciencedirect.com
SCIENCE DIRECT®
Journal of Chromatography A, 1048 (2004) 173–181
JOURNAL OF CHROMATOGRAPHY A
www.elsevier.com/locate/chroma

Continuous desorption rate measurement from a shallow-bed of poly(styrene–divinylbenzene) particles with correction for experimental artifacts

Robert Bujalski, Frederick F. Cantwell*

Department of Chemistry, University of Alberta, Edmonton, Alta., T6G 2G2 Canada

Received 12 May 2004; received in revised form 19 July 2004; accepted 20 July 2004

Abstract

A 0.50 mm high bed, containing ca. 3 mg of the nominally non-porous poly(styrene–divinylbenzene) (PS–DVB) sorbent Hamilton PRP-∞, is located in a valve. After the bed is pre-equilibrated with a (7/3) methanol/water solution of naphthalene (NA), the valve is switched and (7/3) methanol/water solvent flows continuously through the bed at a high linear velocity. This causes NA to desorb into a constantly refreshed solvent, creating a "shallow-bed" contactor with an "infinite bath" kinetic condition. The effluent from the bed passes through a UV-absorbance detector which generates the observed instantaneous desorption rate curve for NA. The same experiment is performed using the solute phloroglucinol (PG), which is not sorbed by PRP-∞ and serves as an "impulse response function marker" (IRF-Marker). The resulting peak-shaped IRF curve is used in two ways (i.e. subtraction and deconvolution) in order to correct the observed instantaneous rate curve of NA for the following experimental artifacts: hold-up volume of the bed and valve, transit-delay time between the bed and the detector and instrument bandbroadening of the NA zone. The cumulative desorption rate curve, which is a plot of moles NA desorbed versus time, is obtained by integration. It is found to be accurately described by the theoretical equation for homogeneous spherical diffusion. The diffusion coefficient of NA inside the PRP-∞ particles $(5.0 \pm 0.6) \times 10^{-11}$ cm^2/s, agrees with the literature value that was obtained from the sorption rate of NA into the same particles. This constitutes virtually conclusive evidence for diffusion control of intra-particle kinetics of NA in the PS–DVB matrix of PRP-∞ and related polymers. The influence of both sorbent and solute properties on the method is evaluated.

Keywords: Desorption rate; Intra-particle diffusion kinetics; Deconvolution; Stationary phases, LC; Polymeric packings; Shallow-bed technique; Naphthalene

1. Introduction

The rates of sorption and desorption into and out of particulate stationary phases contribute to chromatographic band-broadening [1,2]. Any excessively slow sorption/desorption behavior will reduce column efficiencies, yielding broad or even tailed peaks. Slow intra-particle processes can include slow diffusion and/or slow binding and unbinding on the sorption sites. Techniques that have been used to study such intra-particle kinetics include column chromatography [3–11], luminescence methods involving pressure jump [12,13], temperature jump [14] and photon-induced dipole jump [15] and pulsed-gradient spin-echo NMR spectroscopy [16,17].

Uptake-rate and release-rate methods are also used to measure intra-particle kinetics. These methods can be performed in the batch mode either by placing sorbent particles in a stirred solute-containing solution and measuring the depletion of concentration in solution as a function of time, or by placing sorbent particles which have been pre-equilibrated with a solute in a stirred solute-free solvent and measuring the increase of concentration in solution as a function of time [18–22]. In variations of the uptake/release methods a single sorbent particle is contacted with the solution or with the solvent and the concentration of solute in the particle itself is measured as a function of time using microabsorption

* Corresponding author. Tel.: +1 780 492 5927; fax: +1 780 492 8231.
E-mail address: fred.cantwell@ualberta.ca (F.F. Cantwell).

0021-9673/$ – see front matter © 2004 Elsevier B.V. All rights reserved.
doi:10.1016/j.chroma.2004.07.060

spectroscopy [23,24], fluorescence imaging [25] or confocal laser scanning microscopy [26,27].

Uptake/release-rate measurements can also be performed by the shallow-bed technique. To measure the intra-particle sorption rate, sorbent particles are packed into an extremely short column through which a solution of solute is caused to flow at a sufficiently high linear velocity to achieve two conditions [2,20–22,28–35]. The first condition is that the concentration of solute in the solution flowing out of the bed is almost identical to the concentration of solute in the solution flowing into it, so that all particles regardless of their location in the bed are bathed in a solution containing the influent solute concentration at all times. That is, the bed is a "differential contactor" [29,36], also referred to as a zero-length column [37,38]. The second requisite condition is that the Nernst diffusion film [20] of solvent surrounding the particles is thin enough that the time required for diffusion through this film will be negligible compared to the time required for the slow intra-particle process. After a certain time, the flow of solute solution is stopped and the amount of solute that has been sorbed is measured by eluting it out of the particles and performing a quantitative determination on the eluate. The shallow-bed technique is readily performed in the "infinite bath" kinetic mode [20,39] by pumping fresh, rather than recycled [36], solute solution through the bed.

Rate curves have been obtained from shallow-bed measurements for the sorption of naphthalene (NA) by the macroporous poly(styrene–divinylbenzene) (PS–DVB) high-performance liquid chromatography (HPLC) sorbent Hamilton PRP-1 [33,34]. It has been found that these curves accurately predict the contribution of intra-particle kinetics to bandbroadening in the elution chromatography of naphthalene on PRP-1. Rate curves have also been obtained for the sorption of naphthalene by the nominally non-porous PS–DVB sorbent Hamilton PRP-∞. It was shown that the rate of sorption is controlled by diffusion through the polymer matrix [34,35]. A disadvantage of operating in the sorption mode is the labor-intensive and time-consuming nature of the experiments. Each experiment yields the amount of solute sorbed at only a single loading time [2,22,33–35]. The experiment is repeated for different loading times in order to obtain the entire sorption rate curve.

The shallow-bed technique can also be used to measure intra-particle desorption rates. The particle-packed bed is first pre-equilibrated with a solution of the solute and then solute-free solvent is caused to flow through the bed to desorb the solute. By placing a detector downstream of the bed the entire plot of desorbed solute concentration versus time is obtained in one experiment [21,22,28]. The detector signal decays toward zero with time. Reported in the present paper are measurements of the intra-particle desorption rate of naphthalene from spherical particles of the non-porous PS–DVB sorbent Hamilton PRP-∞, performed under shallow-bed, infinite-bath conditions. Emphasis is placed on experimental sources of systematic error and the means by which they can be minimized.

2. Theory

2.1. Rate laws

The detector at the outlet of the shallow-bed reports as a function of time the instantaneous optical absorbance signal $A(t)$ that is produced by the desorbing solute. This absorbance signal is a function of the instantaneous (i.e. differential) molar desorption rate of the solute (dn_i/dt), of the molar absorptivity of the solute ε (L mol^{-1} cm^{-1}), of the pathlength of the detector cell l (cm) and of the flowrate F (L/s) through the bed as shown in Eq. (1):

$$A(t) = \frac{(dn_i(t)/dt)\varepsilon l}{F} \quad (1)$$

In order to transform an experimentally-measured plot of $A(t)$ versus t into a cumulative (i.e. integral) desorption rate curve it is necessary to integrate Eq. (1), as is shown in Eq. (2). Here, $n_i(t)$ is moles of i desorbed by elapsed time t, which increases with time.

$$n_i(t) = \frac{F}{\varepsilon l}\int_0^t A(t)dt \quad (2)$$

2.2. Observed rate curves

In Fig. 1A, an idealized version of the instantaneous rate curve is shown, which can be expected when a shallow-bed, previously equilibrated with solute i, is placed in a flowing stream of eluent. At time zero, solute leaving the bed travels to the detector. Because the flow velocity is necessarily high in order to achieve shallow-bed conditions, the portion of solute which is washed from the extra particle spaces would appear as a very narrow absorbance spike which is labeled as I in Fig. 1A. On the other hand, the portion of solute, which is desorbed from within the particles would appear as a decaying absorbance signal. This is shown as the line bounding the shaded part of Fig. 1A and is labeled as II. Only curve II is related to desorption rate as described by Eq. (1). The more strongly sorbed the solute (larger value of distribution coefficient κ_i) the smaller is the ratio of moles in the spike to moles desorbed.

Fig. 1A is idealized. In reality, the flow of solute between bed and detector requires time and, more importantly, the instrument components through which this flow occurs (e.g. bed outlet frit, connecting tubing, detector cell, detector time constant) produce instrument bandbroadening (i.e. solute zone dispersion) [40,41]. The result of this is the solid line bounding the whole area in Fig. 1B. The part of this plot that is associated with the desorbed portion of solute is shaded, just as it is in Fig. 1A, and it is labeled IV. The part associated with the broadened spike is not shaded and is labeled III.

In order to obtain curve II from the whole of curve (III + IV) in Fig. 1B, the following strategy is employed. The desorption experiment described above is performed also on

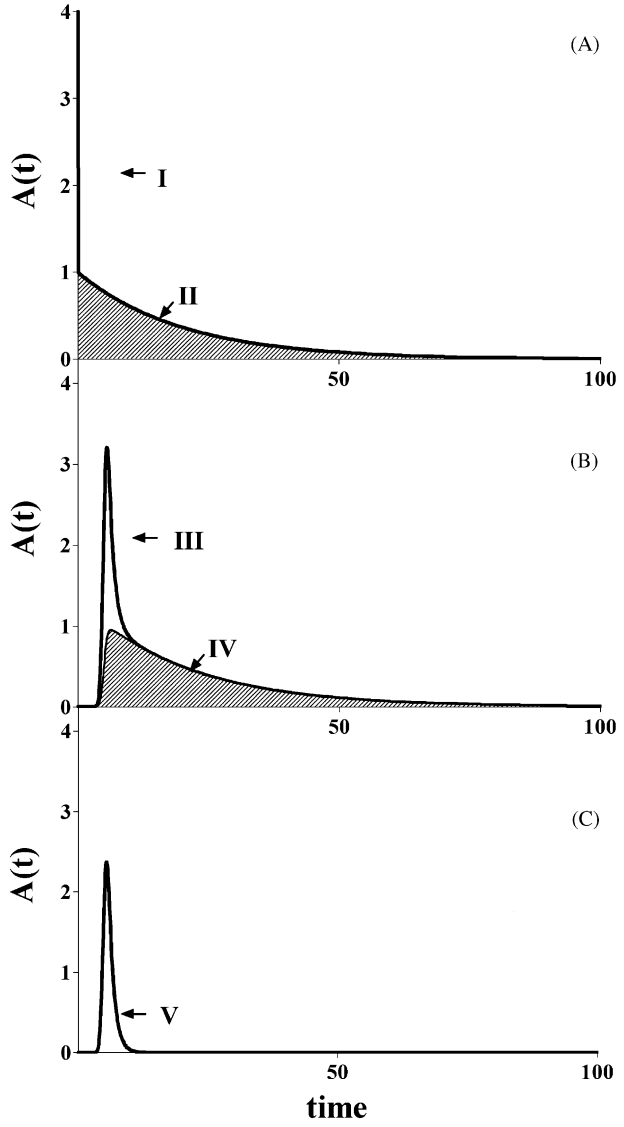

Fig. 1. Simulations of curves associated with continuously monitored instantaneous desorption rate of solute *i* from a shallow-bed. (A) Idealized rate curve including the spike of *i* from extraparticle spaces (I) and the curve for desorbed *i* (II). (B) Observed rate curve showing displacement and band-broadening of the spike (III) and of the desorbed solute *i* (IV). (C) Observed peak for the IRF-Marker (V).

a solute which does not enter the particles in the bed and is not sorbed by them. Such a solute can be called the "impulse response function marker" (IRF-Marker). Shown as the curve labeled V in Fig. 1C is a simulated plot of $A(t)$ versus t such as might be observed for an IRF-Marker. The center of gravity of this somewhat asymmetric peak is displaced from zero along the time axis by the transit time between the bed and the detector. It has a non-zero width as a result of the same instrument bandbroadening processes that are experienced by solute *i*. The IRF peak is used in two ways after its $A(t)$ values are rescaled via multiplication by Eq. (3).

$$\text{Scaling factor} = \frac{V_{hu}[i]_{MP}\varepsilon_i}{V_{hu}[\text{IRF}]_{MP}\varepsilon_{IRF}} \tag{3}$$

In this equation V_{hu} is the hold-up volume of solution between the particles in the bed (it has the same value for both solute *i* and IRF-Marker); ε_i and ε_{IRF} are the molar absorptivities; and $[i]_{MP}$ and $[\text{IRF}]_{MP}$ are the concentrations of solute *i* and of IRF-Marker in the mobile phases that were used to pre-equilibrate the bed and which are therefore present in the hold-up volume at the beginning of the desorption step.

The re-scaled values of the IRF peak are first subtracted from the $A(t)$ values of solute *i* in Fig. 1B at corresponding times. The remaining difference is curve IV. The second use of the IRF peak is to deconvolve curve IV as described in a later section. Deconvolution yields curve II, to which Eq. (1) applies. Finally, integration of curve II according to Eq. (2) gives the experimental cumulative rate curve for solute *i* (not shown in Fig. 1). The resulting curve can then be compared to theoretical kinetic models in order to identify the intra-particle process responsible for the control of desorption rate.

2.3. Theoretical kinetic models

2.3.1. Linear driving force model

Eq. (4) is frequently employed to represent the integral first-order rate equation for sorption and desorption in theories of chromatographic bandbroadening [1,20,42,43]:

$$n_i(t) = n_{i,0}(1 - e^{-kt}) \tag{4}$$

It is a first-order rate equation, which contains a single exponential term. For intra-particle diffusion rate control Eq. (4) can be considered as only a crude approximation of Eq. (5), which contains a sum of many exponential terms. Eq. (4) can be expected to apply when intra-particle rate is controlled by a slow first-order chemical kinetic process such as the site binding step [1]. It is also expected in the case of rate control by extra-particle film diffusion [20].

2.3.2. Spherical diffusion model

Eq. (5) is the theoretical integral rate equation, which describes intra-particle diffusion into and out of a spherical particle [39]. In this equation $n_i(t)$ is both the number of moles of solute that has diffused into the particle by time t during a sorption experiment, and the number of moles of solute that has diffused out of the previously equilibrated particle by time t during a desorption experiment.

$$n_i(t) = n_{i,0}\left(1 - \frac{6}{\pi^2}\sum_{j=1}^{\infty}\frac{1}{j^2}e^{-j^2\beta t}\right) \tag{5}$$

The parameter $n_{i,0}$ is the total number of moles of solute in the particle at sorption equilibrium which can be expressed in terms of the distribution coefficient for the solute κ_i (L/g), the mass of the packing in the shallow-bed, m_{SB} (g) and $[i]_{MP}$ (mol/L).

$$n_{i,0} = \kappa_i[i]_{MP}m_{SB} \tag{6}$$

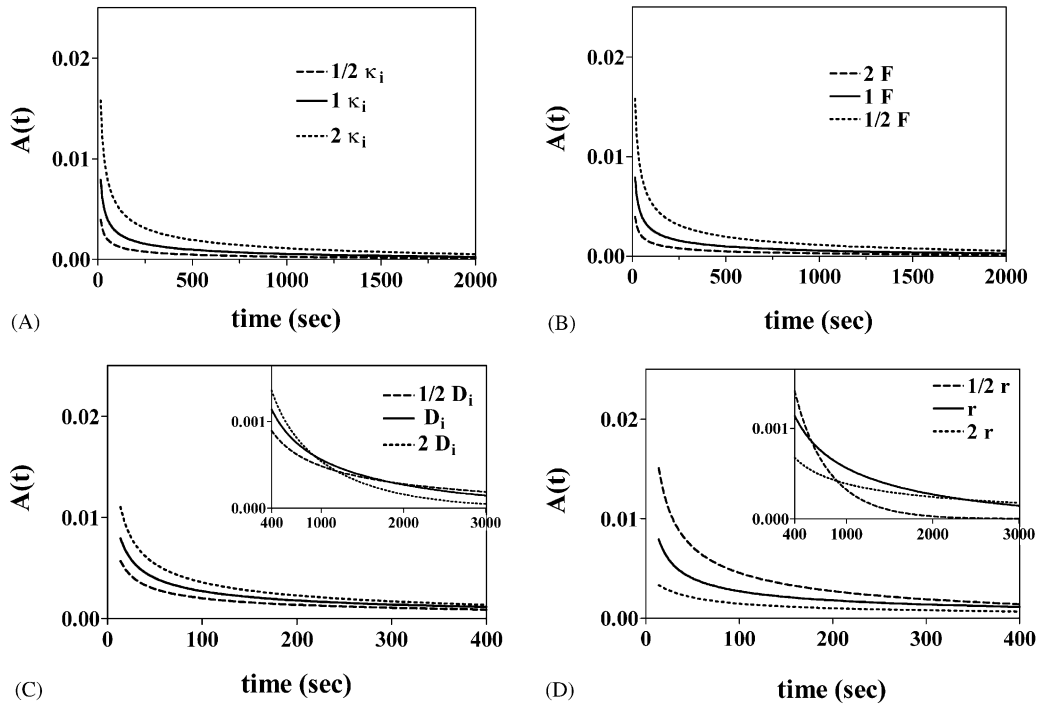

Fig. 2. Predicted effects of varying experimental parameters on instantaneous desorption rate curves calculated with Eq. (8). The parameters with their default values are as follows: (A) κ_i (0.1 L/g), (B) F (0.0833 mL/s through a 0.3 cm diameter bed), (C) D_i (6.0×10^{-11} cm^2/s) and (D) r (1.0×10^{-3} cm). In each panel the solid line is calculated using all default values. Values of non-varied parameters are m_{SB} (2.5 mg); $[i]_{MP}$ (1.6×10^{-4} M); ε_i (5000 M^{-1} cm^{-1}) and detector cell pathlength, l (1.00 cm). Points from the first 15 s of each curve are omitted because only 20 terms were used in Eq. (8).

It is implicit in Eq. (6) that κ_i is constant, which requires that solute i must be present at concentrations in the linear region of its sorption isotherm. The parameter β (s^{-1}) in Eq. (5) is related to the diffusion coefficient D_i (cm^2 s^{-1}) and to the radius of the spherical particle r (cm) as follows:

$$\beta = \frac{\pi^2 D_i}{r^2} \tag{7}$$

If in fact spherical diffusion is the process, which controls the observed, desorption rate then the experimental plot of $n_i(t)$ versus t from Eq. (2) can be fitted with Eq. (5) using non-linear regression. The two fitting parameters are β and $n_{i,0}$.

In order to predict the effects of various experimental parameters on the observed plot of $A(t)$ versus t when spherical diffusion prevails, Eqs. (1), (5) and (6) can be combined to give:

$$A(t) = \frac{6\beta\kappa_i[i]_{MP} m_{SB}\varepsilon_i l}{F\pi^2} \sum_{j=1}^{\infty} e^{-j^2\beta t} \tag{8}$$

Eq. (8), like Eq. (5), contains the sum of an infinite series of exponential terms. The accuracy with which Eq. (8) represents $A(t)$ at shorter and shorter times improves with the number of terms employed. In the present work, the use of the first 20 terms assures that the values of $A(t)$ at and above 15 s time have negligible error. Here, it should be noted that if an infinite number of terms could be used, Eq. (8) would give a numerical value of infinity for $A(t)$ at time zero. This of course is physically impossible since film diffusion is never negligible at very short times [20], so it would become the rate-determining process.

Examples of the predicted effects of various experimental parameters on the instantaneous rate curve are shown in Fig. 2 in which the plots all start at 15 s, as justified by the use of 20 terms in Eq. (8). In Fig. 2A, it is seen that the value of $A(t)$ at any given time is directly proportional to the value of κ_i. The same is true of $A(t)$ with respect to the parameters $[i]_{MP}$, m_{SB}, ε_i and l, all of which appear in the numerator of Eq. (8). In Fig. 2B, it is seen that a slower flow rate gives a larger signal. Although, the area under the curve changes inversely with the flow rate, this change does not reflect the amount of solute in the packing since it is compensated by the presence of F in Eq. (2).

The effects of solute diffusion coefficient (Fig. 2C) and of particle radius (Fig. 2D) are mediated via the parameter β in Eq. (8). A larger value of D_i produces both a higher concentration of desorbed solute and a sharper drop off of $A(t)$ with time. At later desorption times the curves for solutes with higher values of D_i cross over those with lower values since the faster desorption processes decay to zero earlier than the slower ones. This is portrayed in the inset in Fig. 2C. A smaller radius of the packing particles, r, increases β by an inverse square relationship Eq. (7). The resulting effect, shown in Fig. 2D, is more pronounced than that of D_i because r is squared. The area under the $A(t)$ versus t curve is independent of both D_i and r.

Table 1
Parameters from non-linear regression fit of Eq. (5) for spherical diffusion to the cumulative desorption rate curves of NA ($n_{i,0}$ and β are fitting parameters)

Result/parameter	Run 1[a]	Run 2	Run 3	Run 4
m_{SB} ($\times 10^3$ g)	2.53	2.53	2.48	2.48
$[i]_{MP}$ ($\times 10^4$ mol/L)	1.83	1.83	1.36	1.36
F ($\times 10^5$ L/s)	8.58	8.47	7.88	7.88
$n_{i,0}$ ($\times 10^8$ mol)	3.63	4.11	4.05	3.35
β ($\times 10^4$ s^{-1})	5.7	4.6	4.6	5.2
D_i ($\times 10^{11}$ cm^2/s)[b]	5.7	4.6	4.6	5.2
R^2	0.9985	0.9925	0.9982	0.9955

[a] Cumulative rate curve for Run 1 is shown in Fig. 5.
[b] The diffusion coefficient for NA is obtained from β via Eq. (7) using 1.0×10^{-3} cm for particle radius.

3. Experimental

3.1. Reagents, solvents and resin

NA (Coleman and Bell, Norwood, OH) was recrystallized from methanol. Phloroglucinol (PG) (1,3,5-trihydroxybenzene, Fisher) was recrystallized from water. Methanol (MeOH) (certified ACS grade, Fisher) was distilled before use. Water was distilled and deionized with a NANO-pure System (Barnstead, Boston, MA). The eluting solvent, 7/3 MeOH/H_2O, was prepared by combining solvent volumes in this ratio. NA and PG solutions were also prepared in 7/3 MeOH/H_2O with the individual concentrations of NA as given in Table 1. The PG concentration was 11.0 mM. The sorbent PRP-∞ is a nominally non-porous poly(styrene–divinylbenzene) copolymer of particle diameter 19 ± 1 μm [34,35,57] (batch EE2, Hamilton, Reno, NV, USA).

3.2. Apparatus and procedure

3.2.1. Desorption kinetics

Plots of $A(t)$ versus t were measured using the apparatus shown in Fig. 3. Pump P1, which delivers the NA solution, and pump P2, which delivers the eluent, are pulseless constant-pressure pumps operated at 50 psi (3.4 bar) [44]. Pump P3, which delivers the PG solution, is an HPLC pump (Waters 591, Milford, MA). All pumped solutions were thermostated at 25 ± 0.5 °C. The slider valve, V_{SB}, contains the shallow-bed of PRP-∞ (between 2 and 3 mg accurately weighed). It is a modified version of a valve that was previously used in sorption rate studies [33–35]. In the present modification, the left outlet flow channel has been tapered at an angle of 30° from 3.0 mm i.d. to 0.75 mm i.d. starting at a distance 1 cm below the bed. This was done in order to reduce the volume between the shallow-bed and the detector while at the same time maintaining parallel flow streamlines of eluent through the bed during desorption. V_{SB} enables switching of the bed between the loading and the desorption positions.

The NA desorption experiment starts with the slider in the loading position as shown in Fig. 3 in which NA solution passes through the bed for at least 2 h at a flow rate of about 1 mL/min in order unambiguously to establish sorption equilibrium. Meanwhile the eluent solution from P2 passes through the empty hole in the slider valve and flushes out the HPLC detector (Waters Lambda Max 481, 1 cm pathlength, 276 nm wavelength). The detector signal is recorded using a data acquisition program written in Labview on a Pentium 166 MHz PC equipped with a PCI-MIO-16XE-50 input/output board (National Instruments, Austin, TX). The signal gain was 10 in order to decrease the bit noise introduced by the I/O board. After the bed is equilibrated with NA a sequence of three steps requiring 15 s is performed in order to initiate desorption of NA: (i) flows of both NA and eluent are stopped by closing V2 and V3 which are both Cheminert on/off valves (Valco, Houston, Texas, Part #4142410); (ii) the slider in V_{SB} is switched left and (iii) eluent flow from P2 is restarted by opening V3. During desorption the flow rate was measured as the time necessary to fill a specified volume of a burette situated downstream of V3. The major resistance to flow during the desorption step is the detector cell with its connecting tubing. The shallow-bed accounts for about 20% of the total resistance.

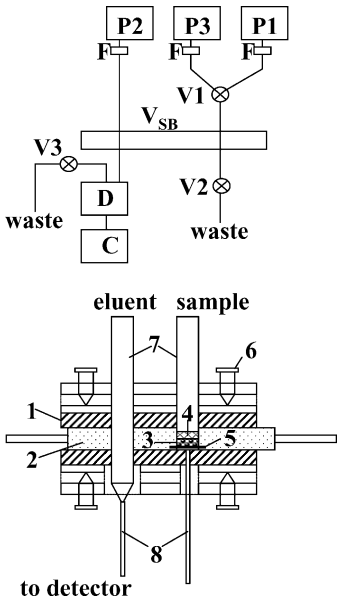

Fig. 3. Top: Schematic diagram of the continuous monitoring shallow-bed desorption apparatus. P1, P2 and P3 are pumps, F is an in-line filter (0.45 μm), V1, V2 and V3 are valves, V_{SB} is the slider valve containing the shallow-bed, D is the detector, C is the computer. Bottom: Schematic diagram of the slider valve V_{SB}. (1) Teflon face plate, (2) Kel-F insert in S.S. slider, (3) bed of PRP-∞, (4) porous Teflon disk, (5) S.S. screen, (6) tension adjustment screw, (7) 3 mm i.d. S.S. tubing and (8) 0.75 mm i.d. (left) and 0.55 mm i.d. (right) S.S. tubing. See text for details.

The PG experiments were performed immediately after the naphthalene experiments using the same sequence of steps with two minor differences. First, the equilibrium (loading) time was only a few minutes since this step had only to ensure that V_{SB} and the tubing were fully flushed. Second, since a constant displacement HPLC pump was used to deliver PG,

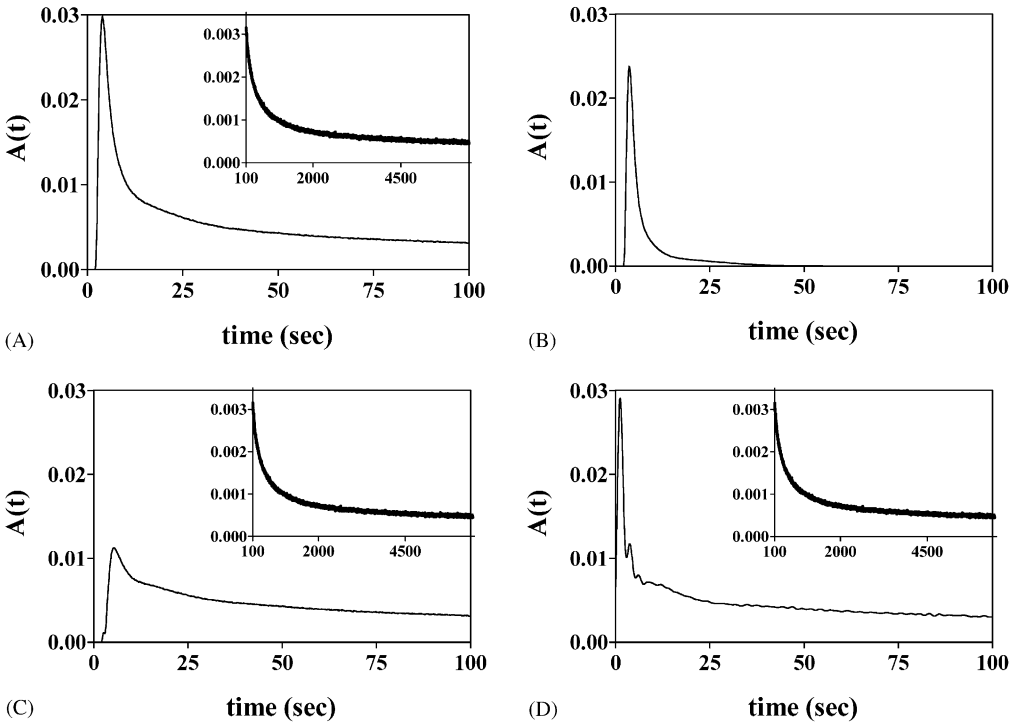

Fig. 4. Instantaneous desorption rate curves for NA (Run 1) and PG. Acquisition frequency was 10 Hz. There are 64,000 data points over the 6400 s. The first 100 s are shown in the large panels, with the remaining 100–6400 s given in the inserts. (A) Observed NA curve, (B) IRF peak for PG scaled by Eq. (3), (C) difference between curves in (A) and (B), and (D) result of deconvolution of curve in (C) with normalized version of curve in (B).

the flow from P3 was stopped and started simply by turning that pump off and on.

The molar absorptivity (ε_i) of NA (5.00×10^3 L mol^{-1} cm^{-1}) in 70/30 MeOH/H_2O was obtained by measuring absorbances of several solutions having concentrations between 1×10^{-6} and 1×10^{-5} mol/L while flowing through the HPLC detector at a flow rate of 5.0 mL/min. The molar absorptivity of PG at 276 nm (262 L mol^{-1} cm^{-1}) was obtained in a separate experiment.

3.2.2. Deconvolution and filtering

The $A(t)$ versus t data for both NA and PG were saved as Microsoft Excel® spreadsheet files. Prior to deconvolution the PG curve in Fig. 4B was normalized to make the area under it equal to 1 (curve not shown). Deconvolution and digital filtering in the Fourier domain were performed by the following steps [45–47]: complex division of the Fourier transform of curve in Fig. 4C by the Fourier transform of the normalized PG curve; multiplication of the quotient of this complex division by the filter function ({0,1}, {0,1}, {0.3,1}, {0.4,0}) [46] in order to remove high frequency noise (>0.4 Hz); and inverse Fourier transformation to produce the deconvolved data in the time domain.

4. Results and discussion

The following topics are considered: the choice of PG as an IRF-Marker, the attainment of shallow-bed conditions, the observed and the corrected instantaneous rate curves, and the cumulative rate curve. The cumulative rate curve is quantitatively interpreted in terms of theory.

4.1. IRF-Marker

Solutes such as NA, which possess a similar solubility parameter to that of the PS–DVB polymer are adsorbed onto the polymer surface and also diffuse into the polymer matrix [34,35,48,49]. In contrast, polar-hydrophilic solutes such as PG neither adsorb onto nor diffuse into a PS–DVB polymer matrix [35]. Furthermore, since PRP-∞ particles are free of meso- and macro-pores, PG cannot enter the particle via that route. Hence, PG meets the IRF-Marker criterion of non-entry into the particles. A secondary criterion is that the IRF-Marker should have a free-solution diffusion coefficient that is similar to that of solute i because free-solution diffusion may be involved in some of the processes that contribute to instrument bandbroadening [41,50–52]. PG is satisfactory also in this regard. The diffusion coefficients for NA and PG at 298 K in 7/3 MeOH/H_2O are 6.0×10^{-6} and 6.9×10^{-6} cm^2/s, respectively, with an estimated uncertainty of 0.7×10^{-6} cm^2/s for each based on calculations employing the Wilke–Chang equation [53].

4.2. Instantaneous rate curve for NA

Data for the first 100 s in a typical experiment on NA (Run 1) and on PG are shown in Fig. 4. The insets show

the remainder of the data from 100 to 6400 s. Fig. 4A is the observed curve of $A(t)$ versus t for the desorption of NA. Fig. 4B is the IRF peak for PG scaled by Eq. (3). Fig. 4C results from subtracting Fig. 4B from Fig. 4A. Fig. 4D shows the result of deconvolution and frequency filtering. In order to clarify their significance, the curves in panels A, B, C, and D of Fig. 4 may be compared, respectively, to the corresponding simulated curves (III + IV), V, IV and II in Fig. 1.

The "ringing" noise, which is evident in the first 100 s of the corrected instantaneous desorption rate curve in Fig. 4D is a common side effect of frequency filtering [54]. Comparison among the curves presented in panels A, C and D reveals that at times longer than about 50 s they are identical to one another (i.e. absorbances at corresponding times agree within 1% relative). This is true for all of the NA runs listed in Table 1. Its significance is that after about 50 s the distorting effects of extra particle NA and of bandbroadening become negligible.

4.3. Shallow-bed and linear isotherm

Ideally, the achievement of shallow-bed kinetic conditions for a desorption process requires that the eluent leaving the bed should contain zero concentration of solute *i*. Of course this condition cannot be met because the desorbed solute molecules produce a non-zero solute concentration in the flowing eluent and furthermore the technique depends on this concentration becoming high enough to be experimentally measurable. In practice, shallow-bed conditions can be closely approximated by ensuring that the maximum solute concentration in the flowing eluent never exceeds a very small fraction of the concentration that was used initially to produce sorption equilibrium (i.e. $[i]_{MP}$ in Eq. (3)). In the present case, $[i]_{MP}$ for the naphthalene loading solution was 1.7×10^{-4} M, while the highest absorbance, observed in curve D of Fig. 4 (i.e. about 0.03 AU), corresponds to a maximum concentration of only 6×10^{-6} M NA in the eluent. After 3–4 s $A(t)$ has become smaller than 0.01 AU which corresponds to a concentration of less than 2×10^{-6} M NA. This is two orders of magnitude smaller than its concentration in the loading solution. Therefore, the requirement of zero solute concentration is effectively achieved after the first few seconds in the present experiments.

The attainment of this condition may also be tested in another way. Eqs. (5) and (8) represent a particular case of a more general zero-length column equation, Eq. (17) in ref. [37], which has been developed for desorption over a broad range of flow-rates. When the parameter L in that equation has a very large value it means that the flow of the mobile phase effectively takes away the desorbing solute as soon as it exits the particle. The average magnitude of L for the present experimental conditions, calculated from Eq. (17) in ref. [37] is 2.1×10^3 which is very large. This is another way of proving that correcting the observed differential desorption rate curve of NA by subtraction and deconvolution with the IRF-Marker effectively eliminates the effect of the holdup volume on the NA curve.

To measure only intra-particle desorption kinetics, the relative rate of diffusion through the Nernst diffusion film surrounding the particle must be much faster than the intra-particle rate. Steady-state diffusion is established across the Nernst film after about 0.01 s in the present system. When intra-particle desorption rate is controlled by diffusion, as is true in this system (see below), the criterion for attainment of exclusively intra-particle rate control is [20]:

$$\frac{[i]_{SP} D_i \delta}{[i]_{MP} D_M r} \ll 0.13 \quad \text{(for particle diffusion control)} \qquad (9)$$

Here, r is the particle radius, δ the film thickness ($\approx$1.6 μm in this case, ref. [20]), $[i]_{SP}$ the equilibrium concentration of solute in the particle in units of mol per litre of particle, and $[i]_{MP}$ is the concentration in units of mol per litre of the surrounding solvent. For NA D_M, the free-solution diffusion coefficient, is 6.0×10^{-6} cm^2/s (see above) and D_i is 5.0×10^{-11} cm^2/s (see below), the density of PS–DVB is about 1 g/mL [55], and the ratio $[i]_{SP}/[i]_{MP}$ is about 100. The left-hand side of Eq. (9) is about 1.3×10^{-4} which is three orders of magnitude smaller than 0.13. This shows that the desorption rate will be controlled by intra-particle processes at times longer than about 0.01 s.

The sorption isotherm of NA from 7/3 MeOH/H_2O onto PRP-∞ is linear with a distribution coefficient of 0.106 L/g up to a solution concentration of about 2×10^{-4} mol/L [35]. Since the loading step of PRP-∞ was done with solutions containing less than this concentration, all experiments were performed in the linear region of the NA isotherm.

4.4. Cumulative rate curve for NA

The instantaneous rate curves (e.g. Fig. 4D) were digitally integrated between 0 and 6400 s for all four experimental runs using Excel software. The average absorbance between 6000 and 6400 s was taken as baseline and the results of the integrations were multiplied by $F/\varepsilon_i l$ in order to obtain the cumulative rate curves for desorption of NA. The curve for Run 1 is shown in Fig. 5 as a solid line which is actually composed of 6400 data points, corresponding to every tenth one of the 64,000 acquired data points. Prism Software Version 4.00 (GraphPad Software, San Diego, CA) was used to fit Eqs. (4) and (5) to all of the points starting at 15 s in these cumulative rate curves using non-linear regression. The regression fit-line of Eq. (4) to the data for Run 1 is shown with a thin dashed line in Fig. 5. Its correlation coefficient (R^2) value is only 0.9601, which indicates a relatively poor fit to the data points. Fits of Eq. (4) to the data for the other three runs yield comparable results (not shown).

The non-linear regression fit-line of Eq. (5) to the data for Run 1 is shown with a thick dashed line in Fig. 5. Fitting parameters $n_{i,0}$ and β and other parameters for all four runs are summarized in Table 1. Correlation coefficients (R^2) are all high suggesting that Eq. (5) describes the data well. The

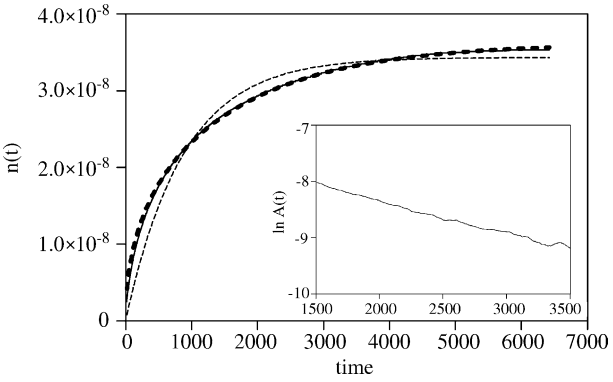

Fig. 5. Cumulative desorption rate curve for NA (Run 1). The apparently solid line is 6400 of the 64,000 experimental points from integration of the points in curve D in Fig. 4 using Eq. (2). The thin dashed line is the regression fit-line for the linear driving force model Eq. (4). The thick dashed line is the regression fit-line for the spherical diffusion model Eq. (5). Inset: a semi-log plot of only the long-time data from the instantaneous desorption rate curve for Run 1 after smoothing and baseline-subtraction. The linear regression fit-line is not shown.

intra-particle diffusion coefficient D_{NA} is obtained from β via Eq. (7). The average value of D_{NA}, with standard deviation, is $(5.0 \pm 0.6) \times 10^{-11}$ cm^2/s ($n = 4$). Comparison of this value via the t-test with the value $(7.1 \pm 0.8) \times 10^{-11}$ cm^2/s ($n = 3$), which previously was obtained from shallow-bed sorption rate experiments [33], shows that these two measured values of D_{NA} are in agreement with one another at the 99% confidence level.

There is an alternative way to obtain D_i which involves using the data from the differential (instantaneous) rate curves such as the one shown in the inset in Fig. 4D. A plot of the natural logarithms of $A(t)$ versus time for only the data at very long times is expected to be linear because Eq. (8) reduces to a single exponential term as the higher order terms become negligible [20,37,38]. The data from Fig. 4D between 1500 and 3500 s, after smoothing by the running average of 100 points and subtracting the baseline absorbance, is presented as the semilog plot in the inset of Fig. 5. The slope of the linear regression line of this plot gives the value of β in Eq. (7), from which D_i can be extracted as described above. The average value of D_i from the four runs is $(5.8 \pm 0.6) \times 10^{-11}$ cm^2/s and the R^2 values for the four runs range from 0.9930 to 0.9962 (inclusion of data much beyond 3500 s would have decreased R^2 for the linear fit due to the lower signal-to-noise ratio and was therefore not included in the semi-log plot). The t-test shows that this average value of D_i agrees with both $(5.0 \pm 0.6) \times 10^{-11}$ and $(7.1 \pm 0.8) \times 10^{-11}$ cm^2/s at the 95% confidence level. It is important to note, however, that there is an advantage to fitting data from the entire cumulative rate curve with Eq. (5) as opposed to fitting only the long-time data with the semi-log plot. A good fit of the entire rate-curve shows that spherical intraparticle diffusion (defined by Eqs. (5) and (8)) is the rate-controlling process, while a good fit to only the data at long times does not. For example, spherical diffusion in a biporous particle is described by an equation containing two diffusion coefficients [34]. Plotting only the long time data would yield only the value of the smaller diffusion coefficient.

The same theoretical spherical diffusion equation describes both the sorption [34,35] and desorption rate curves and in both cases yields the same value for the diffusion coefficient of NA. This result is consistent with the expectation that pure intra-particle diffusion control, free of any significant contribution from film-diffusion control, is the rate-determining process for both sorption and desorption of NA in PRP-∞ in these shallow-bed experiments. The mechanism by which NA diffuses through the PRP-∞ polymer matrix can be treated either as "pore diffusion" through the liquid which fills the micropores, in which case D_{NA} would be an "effective" diffusion coefficient [34], or as diffusive movement among the entangled and crosslinked polymer chains, the structure of which ranges from rigid microporous to soft gel [35]. Previous solvent-sorption and polymer swelling studies would seem to favor the latter [35].

4.5. Minimizing experimental artifacts

Continuous monitoring of the entire time course of desorption of solute from a shallow-bed in a single experiment is convenient. The present work identifies the several artifactual sources of systematic error that cause inaccuracies in this technique and it demonstrates the ways, including deconvolution, in which corrections can be made for them. If these systematic errors cause relatively small distortions of the rate curves as is true in the present case, correction for them in this way yields an accurate corrected rate curve. However, if the systematic errors are relatively much larger it becomes necessary also to reduce their absolute magnitude by modification of the experimental details. For example, this would be necessary in the measurement of desorption rates from HPLC packing materials such as 10 μm diameter particles of an alkylsilyl bonded phase [16,17] for which desorption rates would be much faster (i.e. half-time < 0.5 s) because particle radius is smaller (r in Fig. 2D) and because intra-particle diffusion coefficients are larger (D_i in Fig. 2C). Faster desorption rates give higher concentrations of solute in the early stages of the experiment, which would necessitate the use of higher flow rates (F in Fig. 2B) to attain shallow-bed conditions (i.e. very low concentration of i in the effluent). A higher flow rate and a smaller r both require a higher pump pressure, the latter because the permeability of the bed is inversely proportional to r^2 [55].

Also, for such a packing material the true instantaneous desorption rate curve would be much narrower than the one that is now seen in Fig. 4D and the observed desorption rate curve would be only slightly broader than the IRF peak. This would make it virtually impossible accurately to extract the true rate curve from the observed rate curve solely by deconvolution because of the uncertainty introduced by the unavoidable presence of noise in the data [54]. It would be necessary to reduce instrument bandbroadening by

reducing the volume of the instrument components that are located between the bed and the outlet end of the detector. For porous particles it would be also necessary, in principle, to distinguish the amount of solute in the pores from that between the particles because the former amount should not be subtracted from the observed rate curve. These experimental modifications are all feasible. Their implementation will be the subject of a subsequent report from this laboratory [56] in which are reported desorption rate curves of solute, both from porous 10 μm diameter PS-DVB particles and from porous 12 μm diameter, silica-based, octadecylsilyl (C_{18}) bonded-phase particles.

Acknowledgements

This work was supported by the Natural Sciences and Engineering Research Council of Canada (NSERC) and by the University of Alberta. RB thanks NSERC also for a post-graduate scholarship. Eric Carpenter (Department of Physics, University of Alberta) is gratefully acknowledged for assistance with Labview.

References

[1] J.C. Giddings, Dynamics of Chromatography, Marcel Dekker, New York, 1965.
[2] D. Gowanlock, R. Bailey, F.F. Cantwell, J. Chromatogr. A 726 (1996) 1.
[3] R. Groh, I. Halasz, Anal. Chem. 53 (1981) 1325.
[4] F. Nevejans, M. Verzele, J. Chromatogr. 406 (1987) 325.
[5] V.L. McGuffin, C. Lee, J. Chromatogr. A 987 (2003) 3.
[6] C. Horváth, H.J. Lin, J. Chromatogr. 149 (1978) 43.
[7] A.M. Lenhoff, J. Chromatogr. 384 (1987) 285.
[8] J.C. Giddings, L.M. Bowman, M.N. Myers, Macromolecules 10 (1977) 443.
[9] J.P. Crombeen, H. Poppe, J.C. Kraak, Chromatographia 22 (1986) 319.
[10] J.R. Conder, C.L. Young, Physicochemical Measurement by Gas Chromatography, Wiley, Chichester, 1979.
[11] J.C. Chen, S.G. Weber, Anal. Chem. 55 (1983) 127.
[12] D.B. Marshall, J.W. Burns, D.E. Connolly, J. Am. Chem. Soc. 108 (1986) 1087.
[13] D.B. Marshall, J.W. Burns, D.E. Connolly, J. Chromatogr. 360 (1986) 13.
[14] S.W. Waite, D.B. Marshall, J.M. Harris, Anal. Chem. 66 (1994) 2052.
[15] S.R. Shield, J.M. Harris, Anal. Chem. 74 (2002) 2248.
[16] U. Tallarek, F.J. Vergeldt, H. Van As, J. Phys. Chem. B 103 (1999) 7654.
[17] C.F. Lorenzanoporras, M.J. Annen, M.C. Flickinger, P.W. Carr, A.V. McCormick, J. Colloid Interface Sci. 170 (1995) 299.
[18] D.M. Ruthven, Principles of Adsorption and Adsorption Processes, Wiley, New York, 1984.
[19] M. Suzuki, Adsorption Engineering, Elsevier, Amsterdam, 1990.
[20] F. Helfferich, Ion Exchange, McGraw-Hill, New York, 1962 (Chapters 6 and 9).
[21] A.K. Hunter, G. Carta, J. Chromatogr. A 930 (2001) 79.
[22] R.K. Lewus, F.H. Altan, G. Carta, Ind. Eng. Chem. Res. 37 (1998) 1079.
[23] T. Sekine, K. Nakatani, Langmuir 18 (2002) 694.
[24] K. Nakatani, T. Sekine, Langmuir 16 (2000) 9256.
[25] M.D. Ludes, S.R. Anthony, M.J. Wirth, Anal. Chem. 75 (2003) 3073.
[26] V. Kasche, M. de Boer, C. Lazo, M. Gad, J. Chromatogr. B 790 (2003) 115.
[27] U. Tallarek, M. Paces, E. Rapp, Electrophoresis 24 (2003) 4241.
[28] M. Tetenbaum, H.P. Gregor, J. Phys. Chem. 58 (1954) 1156.
[29] C. Costa, A. Rodrigues, AIChE J. 31 (1985) 1645.
[30] J. Du Domaine, R.L. Swain, O.A. Hougen, Ind. Eng. Chem. 35 (1943) 546.
[31] G.E. Boyd, A.W. Adamson, L.S. Myers Jr., J. Am. Chem. Soc. 69 (1947) 2836.
[32] H. Bieber, F.E. Steidler, W.A. Selke, Chem. Eng. Progr. Symp. Ser. 50 (1954) 17.
[33] J.Y. Li, L.M. Litwinson, F.F. Cantwell, J. Chromatogr. A 726 (1996) 25.
[34] J.Y. Li, F.F. Cantwell, J. Chromatogr. A 726 (1996) 37.
[35] B. Ells, Y. Wang, F.F. Cantwell, J. Chromatogr. A 835 (1999) 3.
[36] M.S. Sanders, J.B. Vierow, G. Carta, AIChE J. 35 (1989) 53.
[37] S. Brandani, D.M. Ruthven, Chem. Eng. Sci. 50 (1995) 2055.
[38] D.M. Ruthven, P. Stapleton, Chem. Eng. Sci. 48 (1993) 89.
[39] J. Crank, The Mathematics of Diffusion, Oxford University Press, New York, 1975.
[40] J.C. Sternberg, in: J.C. Giddings, R.A. Keller (Eds.), Advances in Chromatography, vol. 2, Marcel Dekker, New York, 1966 (Chapter 6).
[41] J. Ruzicka, E.H. Hansen, Flow Injection Analysis, Wiley, New York, 1981.
[42] B. Lin, S. Golshan-Shirazi, G. Guiochon, J. Phys. Chem. 93 (1989) 3363.
[43] S. Golshan-Shirazi, B. Lin, G. Guiochon, J. Phys. Chem. 93 (1989) 6871.
[44] L. Fossey, F.F. Cantwell, Anal. Chem. 54 (1982) 1693.
[45] A. Economou, P.R. Fielden, A.J. Packham, Analyst 121 (1996) 97.
[46] G. Horlick, G. Hieftje, in: D.M. Hercules, G. Hieftje, L.R. Snyder, M.A. Evenson (Eds.), Contemporary Topics in Analytical and Clinical Chemistry, vol. 3, Plenum Publishing Corporation, New York, 1978 (Chapter 4).
[47] T. Yamane, S. Katayama, M. Todoki, Thermochim. Acta 183 (1991) 329.
[48] N. Tanaka, T. Ebata, K. Hashizume, K. Hosoya, M. Araki, J. Chromatogr. 475 (1989) 195.
[49] B.A. Brandrup, E.H. Immergut, Polymer Handbook, Wiley, New York, 1975.
[50] M.J.E. Golay, J.G. Atwood, J. Chromatogr. 186 (1979) 353.
[51] W.N. Gill, V. Ananthakrishnan, AIChE J. 13 (1967) 801.
[52] K.P. Maycock, J.M. Tarbell, J.L. Duda, Sep. Sci. Technol. 15 (1980) 1285.
[53] C.R. Wilke, P. Chang, AIChE J. 1 (1955) 264.
[54] G. Horlick, Appl. Spectrosc. 26 (1972) 395.
[55] U.D. Neue, HPLC Columns: Theory, Technology and Practice, Wiley-VCH, New York, 1997 (Chapter 4).
[56] R. Bujalski, F. Cantwell, University of Alberta, manuscript in preparation.
[57] D. Lee, Personal communication, Hamilton Corp., Reno, NV.